

Article

Comparative Studies of the Structural and Physicochemical Properties of the First Fullerene Derivative FD-C₆₀ (Fullerenol) and Second Fullerene Derivate SD-C₆₀ (3HFWC)

Djuro Koruga ^{1,2,*}, Ivana Stanković ¹ , Lidija Matija ¹, Dietmar Kuhn ³, Bastian Christ ⁴, Sofia Dembski ⁴ , Nenad Jevtić ⁵, Jelena Janać ⁵, Vladimir Pavlović ⁶ and Bart De Wever ⁷

¹ NanoLab, Department of Biomedical Engineering, Faculty of Mechanical Engineering, University of Belgrade, 11220 Belgrade, Serbia; imileusnic@mas.bg.ac.rs (I.S.); lmatija@mas.bg.ac.rs (L.M.)

² NanoWorld, 11043 Belgrade, Serbia

³ LAUS GmbH, 67489 Kirrweiler, Germany; dietmar.kuhn@laus.group

⁴ Fraunhofer, Institute for Silicate Research ISR, 97082 Würzburg, Germany; bastian.christ@isc.fraunhofer.de (B.C.); sofia.dembski@isc.fraunhofer.de (S.D.)

⁵ TFT Nano Centre LLC, 11010 Belgrade, Serbia

⁶ TEM Laboratory, Faculty of Agriculture, University of Belgrade, 11000 Belgrade, Serbia; vlaver@agrif.bg.ac.rs

⁷ Altexa Development, 98000 Monaco, Monaco

* Correspondence: dkoruga@mas.bg.ac.rs or djuro.koruga@gmail.com

Abstract: In order to maximally reduce the toxicity of fullerenol (the first derivative of C₆₀, FD-C₆₀), and increase its biomedical efficiency, the second derivative SD-C₆₀ (3HFWC, Hyper-Harmonized Hydroxylated Fullerene Water Complex) was created. Several different methods were applied in the comparative characterization of FD-C₆₀ and SD-C₆₀ with the same OH groups in their core. FD-C₆₀ as an individual structure was about 1.3 nm in size, while SD-C₆₀ as an individual structure was 10–30 nm in size. Based on ten physicochemical methods and techniques, FD-C₆₀ and SD-C₆₀ were found to be two different substances in terms of size, structure, and physicochemical properties; FD-C₆₀, at 100 °C, had endothermic characteristics, while SD-C₆₀, at 133 °C, had exothermic characteristics; FD-C₆₀ did not have water layers, while SD-C₆₀ had water layers; the zeta potential of FD-C₆₀ was –25.85 mV, while it was –43.29 mV for SD-C₆₀. SD-C₆₀ is a promising substance for use in cosmetics and pharmaceuticals.

Keywords: fullerene C₆₀; first derivate C₆₀; second derivate C₆₀; TEM; AFM/MFM; NMR; XRD; TGA/DTA-MS-FTIR; zeta potential; endothermic/exothermic properties



Citation: Koruga, D.; Stanković, I.; Matija, L.; Kuhn, D.; Christ, B.; Dembski, S.; Jevtić, N.; Janać, J.; Pavlović, V.; De Wever, B.

Comparative Studies of the Structural and Physicochemical Properties of the First Fullerene Derivative FD-C₆₀ (Fullerenol) and Second Fullerene Derivate SD-C₆₀ (3HFWC).

Nanomaterials **2024**, *14*, 480. <https://doi.org/10.3390/nano14050480>

Academic Editor: Mohammed Jaouad Meziani

Received: 2 February 2024

Revised: 22 February 2024

Accepted: 5 March 2024

Published: 6 March 2024



Copyright: © 2024 by the authors. Licensee MDPI, Basel, Switzerland. This article is an open access article distributed under the terms and conditions of the Creative Commons Attribution (CC BY) license (<https://creativecommons.org/licenses/by/4.0/>).

1. Introduction

Since their discovery about 45 years ago, fullerenes and their physicochemical properties and applications have attracted the attention of researchers. This carbon-based nanomaterial, particularly fullerene C₆₀, has captured the extra attention of scientists due to its symmetry and physicochemical properties. Fullerene C₆₀, as a molecular crystal, was predicted by Osawa [1], synthesized and identified using mass spectroscopy by Kroto et al. [2], produced in gram quantities by Huffman et al. [3], and viewed at atomic resolution using a scanning tunneling microscope (STM) by Koruga et al. [4]. It has a high icosahedral symmetrical arrangement of carbon atoms, and their eigenvalues T_{1g}, T_{2g}, T_{1u}, and T_{2u} have four Fibonacci values $1/2(1 + \sqrt{5})$, $-1/2(1 + \sqrt{5})$, $1/2(1 - \sqrt{5})$, and $-1/2(1 - \sqrt{5})$, respectively, (Φ , $-\Phi$, $-\phi$, and ϕ , respectively, in Table S1). The rotation–vibration spectra of the C₆₀ icosahedral molecule has been investigated [5], and its dual particle–wave properties have been experimentally discerned [6]. Since then, some biomolecules, such as clathrin, microtubules, etc., have been shown to have similar icosahedral symmetry properties [7,8] to SD-C₆₀, which allows them to establish a resonant

interaction with SD-C₆₀. This is possible because the electronic and vibrational states of biomolecules are determined by their symmetry, and the vibrational modes of SD-C₆₀ can be resonantly transmitted to biomolecules and influence them.

Fullerene C₆₀ is a spherical molecular crystal with 60 carbon atoms distributed over the surface of the sphere in 12 pentagons and 20 hexagons [2]. Pentagons are energetically closed structures (diamagnetic), while hexagons are open-closed structures that “breathe” (paramagnetic) [9].

Due to its physical properties, based on symmetry, C₆₀ is not soluble in water. It can become toxic when it comes under the influence of external factors, which lead to the opening of one of the two (C=C) bonds in the hexagons. The first fullerene derivative, FD-C₆₀ (commercially named fullerol C₆₀(OH)_x), was synthesized by adding OH groups in order to achieve water solubility as well as to reduce possible toxicity [10]. Water solubility depends on the number of OH groups, which can be different; however, the stability of fullerol has proven to be the best if it has 12, 24, 36, or 48 OH groups. Since the diameter of the C₆₀ molecule, at the position of the carbon atom, is 0.71 nm, and the outer diameter is about 1 nm (due to π -electrons), the diameter of fullerol is roughly 1.3 nm with the addition of the OH groups. It has been shown that the toxicity of C₆₀ is reduced by 50% if OH groups are added [11]. Fullerene hydroxylation increases water solubility and affects how these nanoparticles interact with biological systems. It has been demonstrated that increasing fullerene water solubility through surface modification is related to significantly decreased toxicity. Specifically, this study observed decreased toxicity of hydroxylated fullerene compared to the cytotoxic effects of fullerene aggregates in human skin (HDP) and liver carcinoma (HepG2) cells [11]. Similarly, it was observed that hydroxylation decreases the toxic potential of fullerene in mouse L929 fibrosarcoma, rat C6 glioma, and U251 human glioma cell lines [12]. Additionally, hydroxylated fullerene induced apoptotic changes in the investigated cell lines, while fullerene C₆₀ induced necrotic cell death. The distinct effects of pristine and modified fullerene originate from the different nanoparticle interactions with the intracellular metabolic pathways [11,12].

The beneficial effects of fullerol are well documented. In human breast cancer cell lines, C₆₀(OH)₂₂ inhibited cancer cell growth and suppressed doxorubicin-induced cytotoxicity [13]. In a study by Jiao et al. [14], fullerol C₆₀(OH)₂₀ showed antitumor and antimetastatic activity in an in vivo EMT-6 breast cancer metastasis model. The antitumor effect of fullerol C₆₀(OH)₂₀ may be exerted through its effects on oxidative stress status, inhibition of the formation of angiogenesis factors, or through modulation of the immune profile [15].

However, fullerene hydroxylation did not provide the absolute absence of toxicity in living systems [16,17]. Additionally, the degree of fullerene hydroxylation affects toxicity [18,19]. Therefore, the physicochemical properties of fullerene derivatives are of prime importance for achieving optimal effects in living systems.

In order to further reduce its toxicity or even completely eliminate it, as well as to improve the transfer of the C₆₀ vibrational modes to biological water and biomolecules, the second derivative of C₆₀, SD-C₆₀ (C₆₀(OH)₃₆•(H₂O)₁₄₄₋₂₅₂₈), commercially named 3HFWC—Hyper-Harmonized Hydroxylated Fullerene Water Complex, was designed, synthesized and tested [20–22]. In reference [22], an explanation of the creation of stable water layers around FD-C₆₀ (fullerol) and obtaining SD-C₆₀ (3HFWC) as three-dimensional Penrose tilings (3DPTs) is given. This was achieved by sequentially changing the angle between the hydrogen bonds in the water molecules according to the Fibonacci sequence of the Φ number, i.e., by the eigenvalues of T_{1u}, T_{2u}, T_{1g}, T_{2g} of icosahedral symmetry. This was the first time the angle between the hydrogen bonds in the water molecules was sequentially changed according to the sequence of Φ (3/2 = 1.5, 5/3 = 1.66, 8/5 = 1.60, 13/8 = 1.625, 21/13 = 1.615, 34/21 = 1.619, 55/34 = 1.617, 89/55 = 1.618, 144/89 = 1.617...). The experimental results showed that the stability of this change in water layers was stable for at least three years. This new technology of packing water molecules into 3D Penrose tiles with icosahedral symmetry enabled water to exert its biophysical effect on biomolecules

without the need for biochemical reactions. Therefore, this could be the beginning of a new direction in medicine, which we can call “water-based nanomedicine”.

Experimental results with SD-C₆₀ (3HFWC) in the field of biomedicine, agriculture, and cosmetics have shown desirable effects. Specifically, effects on melanoma [22–24], an influence on Alzheimer’s disease [25], a reduction of pain and improved memory in mice [26], the formation of hydrogen peroxide in tomatoes, and an increase in lycopene and regulation on the flow of water from the extracellular space into the cell [27]. Most of the current methods and techniques in the fight against cancer are of a destructive nature, destroying diseased cells, and therefore also healthy ones that are in the immediate environment. The SD-C₆₀-based method works differently. It was found that SD-C₆₀ (3HFWC) realized its anti-melanoma action through initiation of cell reprogramming, demonstrating senescence establishment and a minor contribution to cell death. Our goal was to show that we had developed a substance different from fullerol capable of reprogramming malignant cells rather than causing tumor cell death, which thus might have serious consequences on proliferation.

Additionally, the beneficial effects of skin hydration, synthesis of collagen and elastin, and biophysical properties of the human skin were demonstrated [28,29].

Bearing in mind the increasing interest for the application of both FD-C₆₀ (fullerol) [13–19,30–38] and SD-C₆₀ (3HFWC) [22–29] in biomedicine and cosmetics, it is necessary to present a comparative physicochemical characterization of them. There are several studies that present the physicochemical characteristics of fullerol [39–42], but since fullerol can have a different number of OH groups (usually from 12 to 48), there can be significant differences in the properties of fullerol. For this reason, this paper characterizes fullerol (FD-C₆₀), which is a precursor to the second derivative of C₆₀, SD-C₆₀ (3HFWC), i.e., with the same number of OH groups. In order to determine size, stability, exothermic and endothermic properties, spectral characteristics, and the existence of water shells (layers), research concerning FD-C₆₀ and SD-C₆₀ in solution and in a dry state was carried out in several laboratories across Europe, using devices such as AFM/MFM, TEM/STEM, ¹³C-NMR, ¹H-NMR, GPC, ZetaPro, XRD, TGA/DTA, UV-vis-NIR, and FTIR spectrometers [43–53]. The experiment design is given in the Section 2; it was performed in such a way that by characterizing both of these nanomaterials, their main physicochemical properties could be obtained. On this basis, the conclusions could be drawn about their similarities and differences. This complex comparative approach was applied for the first time to FD-C₆₀ (fullerol) and SD-C₆₀ (3HFWC), and the data have been made available to the scientific community.

2. Materials and Methods

2.1. Samples Preparation

The fullerol (C₆₀(OH)₃₆) or FD-C₆₀, with a molecular weight of 1332 Da, a dust composition (yellow color), and a purity of 99.99% (as a precursor of SD-C₆₀), was ordered in a dark bottle from Solaris Chem, Vaudreuil-Dorion, QC, Canada. It was stored in a dark room, with a humidity of 35 ± 2% and a temperature of 20 ± 2 °C.

The SD-C₆₀ (C₆₀(OH)₃₆)@(H₂O)_{144–2528} or 3HFWC, with a molecular weight of 3.826–47.124 Da, was synthesized at the TFT NanoCenter, Belgrade, Serbia (3 g of fullerol was mixed with 20 L of ultra-pure water for commercial use), according to the patented procedure [20,21]. The formation of SD-C₆₀ began with 0.150 g/L of hydroxylated fullerene C₆₀(OH)₃₆ dissolved in high-purity water (0.05 µS/cm) under the influence of an external oscillatory magnetic field +250/–92 mT according to the icosahedral eigenvalues T_{1g}, T_{2g}, T_{1u}, and T_{2u} (Fibonacci numbers Φ, –Φ, –ϕ, and ϕ). At the same time, under the internal action of the vibrations of the C₆₀ molecules (same vibration law as an external magnetic field) in a reactor at 37 °C, the formation of 3HFWC was realized [22]. The composition of SD-C₆₀ (3HFWC) was as follows: (1) solid-state of 2.5–3%, (2) ordered water in chains (crystalline, linear chains between the solid-state 3HFWC units) 58–60%, (3) fullerol (around which water layers failed to form) about 0.05%, and (4) free water about 38% [22].

The SD-C₆₀ solid-state of 2.5–3% was the dry residue value obtained from the solution when dried immediately before the characterization experiments. The SD-C₆₀ was stored in a dark bottle, in a dark place, at a room humidity of 35 ± 2% and a temperature of 20 ± 2 °C. In relation to when the SD-C₆₀ solutions were produced, there were three solution samples: three years old, two years old, and eight months old. Investigations of SD-C₆₀ in solution were carried out using UV-vis–NIR, FTIR, ZetaPro (Doncaster, UK), and GPC techniques, while dried SD-C₆₀ (solid-state) was investigated using TEM/STEM, AFM/MFM, XRD, TGA/DTA-MS-FTIR and NMR techniques. Dry samples of SD-C₆₀ were made immediately before the experiment; it was also recorded how long the solid form of SD-C₆₀ could survive in solution (Table S2).

2.2. UV-vis–NIR and FTIR

UV-vis–NIR characterization of both FD-C₆₀ (fullerol) and SD-C₆₀ (3HFWC) was performed using a Lambda 500 spectrometer, Perkin-Elmer, USA, in the range of 250–3000 nm. FTIR characterization of both FD-C₆₀ (fullerol) and SD-C₆₀ (3HFWC) was performed using the Spectrum Spotlight 400 FTIR Imaging System, Perkin-Elmer, Waltham, MA, USA, in the range of 2500–14,000 nm. Additionally, the following instruments were used for the characterization: near-infrared spectrometer Lambda 1050+, Perkin Elmer, up to 2600 nm; Infrared Spectrometer Spectrum Two FT-IR, Perkin Elmer; Laser HeNe Class 1, with a scanned range of 370–7800 cm⁻¹; UV-vis spectrometer Specord 205, Analytik Jena (Jena, Germany), with a resolution of ±0.5 nm and a scanned range of 190–1100 nm.

2.3. TEM and HAADF-STEM

Transmission electron microscopy (TEM) analysis of the dry particles of both FD-C₆₀ (fullerenol) and SD-C₆₀ (3HFWC) was performed in order to determine their solid-state size. The samples in a liquid state were applied to the TEM copper mesh coated with carbon and dried in air. After drying the samples, they were analyzed and recorded in three TEM laboratories: (1) the CM12 Philips/FEI Transmission Electron Microscopy, Eindhoven, the Netherlands, magnification ×45,000 and ×60,000 (solution was 6 months old); (2) TEM, JEM 1400, JEOL, Tokyo, Japan, magnification ×120,000 up to ×200,000 (solutions were 8 months old and 3 years old); and (3) High-Angle Annular Dark Field Scanning Transmission Electron Microscopy (HAADF-STEM), Thermo-Fisher Talos/Osiris 200 kV (Waltham, MA, USA), Zeis Libra (Oberkochen, Germany) 120 kV, 200 kV electron energy, STEM mode with bright field, with evaluation software Thermo-Fisher Velox 3.7 and energy-dispersive X-ray analysis EDXS mapping = ChemiSTEM, with Z > 8 installed (the solution sample was 8 months old).

2.4. AFM/MFM

AFM/MFM characterization of FD-C₆₀ and SD-C₆₀ was performed after drying the samples on copper coated with carbon; the samples (solution was 8 months old) were stored in dark, closed containers and kept at room temperature until use. Characterization of the dry samples was performed using a JSPM-5200, Scanning Probe Microscope, JEOL, Tokyo, Japan. Two methods were used: AFM (atomic force microscopy) and MFM (magnetic force microscopy). Both techniques are non-invasive methods: the AFM method is based on van der Waals forces and London-type dispersive forces between the tip and sample; while MFM, in the non-contact imaging mode, is based on magnetic dipole–dipole interactions between the tip and sample (measuring ± deflection of the tip “φ” in degrees). For the purpose of investigating the magnetic gradient, specialized cantilevers, type HQ NSC18/Co-Cr Al BS (Micro Mash, Tallinn, Estonia), with a force constant between 1.2 and 5.5 N/m and a resonant frequency range from 60 to 90 kHz were used. Scan sizes at 30 nm, 100 nm, and 300 nm were performed.

2.5. XRD

Powder X-ray diffractograms (XEDs) were recorded on a Rigaku (Woodlands, TX, USA) SmartLab 3 kW from 5 to 85° 2Theta at room temperature. For preparation, an aqueous 3HFWC solution was lyophilized for 7 days to give a brownish powder. Fullerol was used as a powder, as delivered from Solaris Chem, Canada.

2.6. TGA/DTA-MS-FTIR

TGA/DTA-MS-FTIR measurements were performed on an STA 449C Jupiter (TGA/DTA) and an Aeolos QMS 403 C (MS) from Netzsch, Germany, and a Bruker Tensor 27 (Billerica, MA, USA) with a gas chamber (FTIR). Lyophilized 3HFWC and fullerol dried under vacuum (10 mbar/30 °C) were weighed in Al₂O₃ crucibles. During the measurements, the samples were heated from 30 to 900 °C with a constant heating rate of 10 K/min under a synthetic air atmosphere.

2.7. ¹³C-NMR and ¹H-NMR

The Avance DRX 400, Bruker, BioSpin GmbH Cryo, at frequencies of 400 MHz (¹H) and 100 MHz (¹³C), and a temperature of 300 K, was used with a solution-saturated solution. The sample was dissolved in D₂O, and ¹H and ¹³C spectra were recorded. ¹H-NMR spectra were recorded with water suspension, while ¹³C-NMR spectra were recorded with water suspension without TMS.

2.8. Zeta Potential

The zeta potential was recorded via electrophoretic light scattering using the BeNano 180 ZetaPro analytical instrument. Sample preparation was as follows: the roller mixer was set at a measuring temperature of 25 °C, cell measurements were performed using the folded capillary cell, with five repetitions of the fold measurements and evaluation of the mean value from five measurements.

2.9. GPC

For gel permeation chromatography, we used the following: precolumn PSS Suprema: 5 µm, Guard, ID 8.0 mm × 50 mm; PSS Suprema: 5 µm, 30 Å, ID 8.0 mm × 300 mm PSS Suprema: 5 µm, 1000 Å, ID 8.0 mm × 300 mm; PSS Suprema: 5 µm, 1000 Å, ID 8.0 mm × 300 mm; Pump PSS SECurity 1260 HPLC-pump, Agilent, Burladingen, Germany: flow rate of 1.0 mL/min, injection volume of 100 µL, and temperature 35 °C; detectors PSS SECurity refractive detector (RI); PSS SECurity ultraviolet light detector (UV); and Calculation PSS-WinGPC Unity Version 8.4. Sample preparation for gel permeation chromatography (GPC) was based on a procedure where the received sample solutions were transferred into the injections vials and injected by an autosampler without any further pre-treatment. Several pullulan standards with different molecular weights were measured to construct a calibration curve. The calculation of the average molecular weights and the molecular weight distribution of the samples was performed using the so-called “slice-by-slice” method based on the pullulan calibration.

3. Results

Since two spectroscopic domains, 2500–3300 nm and 6000–7000 nm, were important for fullerol and 3HFWC application in biomedicine, we begin with the presentation of the similarities and differences between them from our results. The first spectral domain is important for the organization of water molecules into water layers (shells), while the second domain is important for the biophysical influence of the first and second C₆₀ derivatives on biomolecules. Beside water (...H-O-H...O-H...O-H...) and DNA (A=T, C≡G), the amide-I (...H-N-C=O...H-N-C=O...) hydrogen bonds have a very important role in the secondary structure of biomolecules (proteins), their stability, conformation states, and functionality.

3.1. NIR and FTIR Spectroscopy

FD-C₆₀ (fullerenol with an average of 36 OH groups, Figure S1) had one peak at 3088 nm with low intensity (0.05 a.u.), which means that it contained OH groups and had hydrogen bonds connected to water molecules from the humidity level (Figure 1). There were also three more peaks at 6377 nm, 7562 nm, and 12,865 nm with peaks intensity of 0.20, 0.17, and 0.13 a.u., respectively, that could affect biomolecules via their vibrational modes.

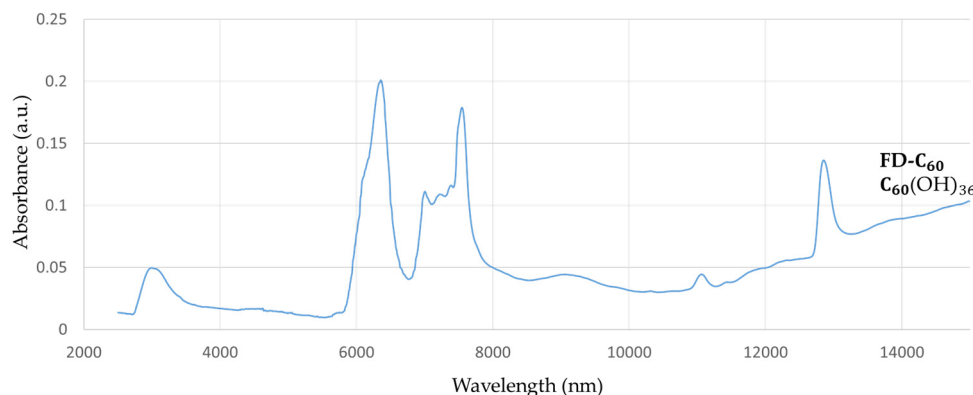


Figure 1. The FTIR spectrum of fullerol (FD-C₆₀) in the 2500–15,000 nm domain. There are four dominant peaks, one at 3088 nm (spontaneously water shell around FD-C₆₀) with an intensity of 0.05 a.u., one at 6377 nm with an intensity of 0.20 a.u., one at 7562 nm with an intensity of 0.17 a.u., and one at 12,865 nm with an intensity of 0.13 a.u.

SD-C₆₀ (3HFWC, whose precursor is fullerol with 36 OH groups) had a peak at 3064 nm with an intensity of 0.28 a.u., which showed that due to the OH groups, water from the humidity level also had water layers (Figure 2). In addition, there was a peak at 6132 nm with an intensity of 0.14 a.u., and an elevated area from 10,000 nm to 15,000 nm with intensities of 0.05 a.u. and 0.35 a.u., respectively.

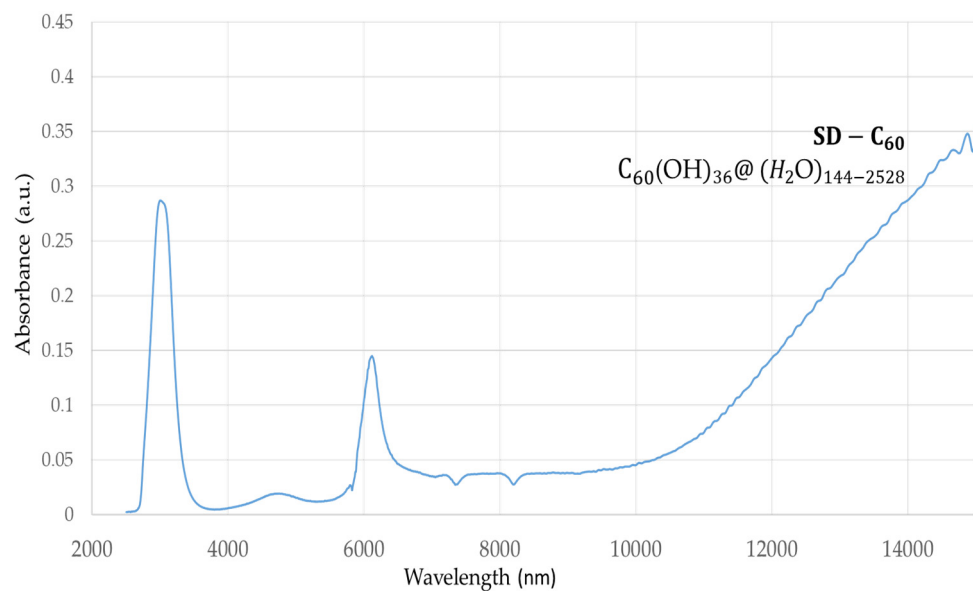


Figure 2. FTIR spectrum of 3HFWC (SD-C₆₀) in the 2500–16,000 nm domain. There are two dominant peaks at 3064 nm (intramolecular “chelate” hydrogen bonds) with an intensity of 0.28 a.u., and 6132 nm with an intensity of 0.14 a.u. Furthermore, the spectrum exhibits an increasing value of 0.05–0.35 a.u. in the 10,000–15,000 nm domain, with a peak in this area above 15,000 nm (could not be detected because it was outside the instrument’s wavelength domain).

If the peaks from Figures 1 and 2 are compared at around 3000 nm, it can be seen that the peak with 3HFWC was five to six times more intense than with fullerol. This result shows that there are many more hydrogen bonds in 3HFWC than in fullerol. Concerning the nature of the intramolecular water hydrogen bonds, they first formed rings on the surface of the sphere (“chelate”) and then ordered themselves into a closed water shell as three-dimensional Penrose tiles [22]. The $C_{60}(OH)_n$ replaced the ion role (in the classical sense) in the center of the coordinate bonds; this is the reason why “chelate” is written in quotation marks. As fullerol ($C_{60}(OH)_n$) is a precursor of 3HFWC, when we subtracted the intensity of the fullerol peaks from the 3HFWC peaks, we obtained the peak intensities of only the hydrogen bonding water shells (layers) of 3HFWC, which was 0.23 a.u. Additionally, a big difference in the peak intensity of about 0.22 a.u. was within the 10,000–15,000 nm range, which gives a two to seven times higher intensity value of the effect on biomolecules.

3.2. ^{13}C -NMR and 1H -NMR

The characterization results of fullerol and 3HFWC using ^{13}C -NMR and 1H -NMR showed similarities and differences between these two substances (Figures 3 and 4). The ^{13}C -NMR spectrum of fullerol had peaks from 172 to 181 ppm (the number of OH groups were 32, 36, 44, and 48, with a dominant peak at 176.49 ppm, i.e., 36 OH groups); signals (126–138 ppm) showing C=C bonds in the C_{60} molecule and C-O-H bonds (75,25 ppm) were observed. Having in mind that the intensity for 36 –OH groups was much higher, it can be concluded that the most abundant number of –OH groups was 36 (Figure S3).

As can be seen, no single peak was observed in the ^{13}C -NMR spectrum of 3HFWC. This indicates two possibilities; either the ^{13}C signal was so weak (in nature, only 1.1% of carbon atoms are ^{13}C) that the device could not detect it or the 3HFWC water layers absorbed the ^{13}C magnetic signal. Bearing in mind that the same fullerol material was used in both cases at the same concentration (0.150 g/L), we are more inclined to think that the ^{13}C signal was absorbed by the water layers rather than not being detected due to weakness. However, in order to provide a valid conclusion, it is necessary to do additional research.

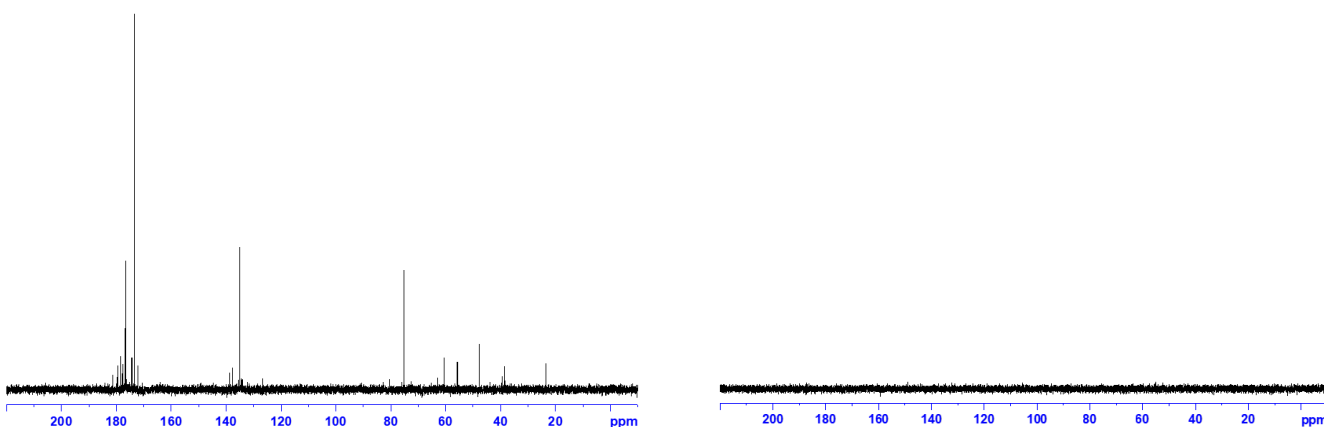


Figure 3. (Left) ^{13}C -NMR spectrum with a water suspension of fullerol (FD- C_{60}) at a concentration of 0.15 $\mu\text{g}/\mu\text{L}$. Thirteen peaks from 172 to 181 ppm show the different forms of fullerol (from 30 to 50 OH groups), with a dominant peak at 176.49 ppm (36 OH groups). The second peak from 126 to 138 ppm show C=C bonding in C_{60} , while the peak at 75.25 ppm represents a C-OH group in the hydroxylated fullerene. **(Right)** ^{13}C -NMR spectrum with a water suspension of 3HFWC (SD- C_{60}) at the same concentration of fullerol (0.15 $\mu\text{g}/\mu\text{L}$, as a precursor). ^{13}C -NMR could not detect peaks of ^{13}C atoms despite using the same concentration as in the fullerol experiments. We assume that there are two possible reasons for this: (1) too few ^{13}C atoms in the sample to detect a signal, or (2) the water layers of 3HFWC absorbed the magnetic signal of ^{13}C atoms.

¹The H-NMR spectra, both ppm and integral, of fullerol and 3HFWC without TMS are presented in Figure 4 and Table 1.

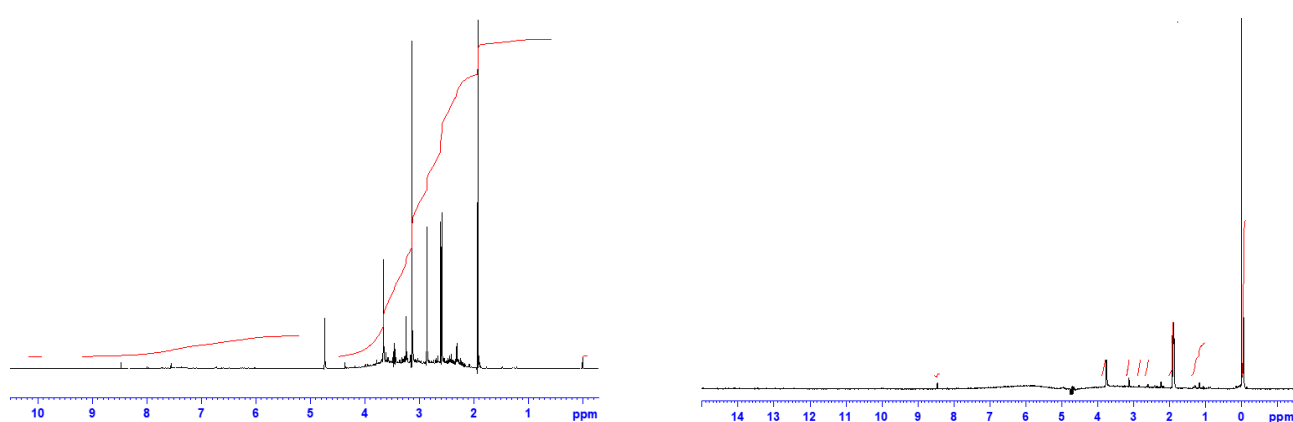


Figure 4. ¹H-NMR spectra of fullerol (FD-C₆₀) with six dominant peaks from 4.8 ppm to 1.9 ppm (**left**), and 3HFWC (SD-C₆₀) with three dominant peaks from 0 ppm to 3.8 ppm (**right**). The black lines represent a chemical shift (ppm), while the red lines represent the integral spectra.

Table 1. Differences between fullerol and 3HFWC based on the ¹H-NMR spectra (chemical shift/ppm and integral difference without TMS). The difference in the chemical shift is small, about 0.3 ppm, while the integral value is significantly different, about 4.3 times.

3HFWC without TMS Chemical Shift/ppm	3HFWC without TMS Integral	Fullerol without TMS Chemical Shift/ppm	Fullerol without TMS Integral
8.459	3.57	8.765–4.811	15.31

A significant chemical shift was seen in the 3HFWC ¹H-NMR spectrum (without TMS) at 8.45 ppm, while fullerol had many peaks between 8.76 and 4.81 ppm. The integral spectrum of 3HFWC had a value 3.57, while fullerol had a value of 15.31. These structures and values tell us that protons in 3HFWC have a higher symmetrical order than fullerol (Figure S4).

3.3. TEM Images

TEM images of dry fullerol and dry 3HFWC were taken in three independent laboratories. Samples of the 3HFWC solutions, before drying, and from eight months to three years old, were sent. Information regarding the age of the solution concerned the stability of 3HFWC (soft solid state, which becomes a dry residue during drying) in the given solution. Fullerol was prepared as a solution and dried just before the experiments.

TEM characterization showed that fullerol had a diameter of 2.0 ± 0.6 nm (Figure 5, left) and could be clustered under humidity, forming large agglomerates (a few hundred nanometers) with a molecular weight between 1230 and 1536 Da (average 1332 Da). In theory, fullerol is about 1.3 nm, which indicates that at room temperature and normal room humidity 35–45%, fullerol is organized as a monomer (1.3 nm) or a dimer (2.6 nm).

All three TEM laboratories (two at the University of Belgrade and one at LAUS, Germany) obtained similar results for dry 3HFWC (SD-C₆₀). Dry 3HFWC showed a spherical nanoparticle structure of sizes 10 nm–30 nm (Figure 5, right, and Figures 6 and 7).

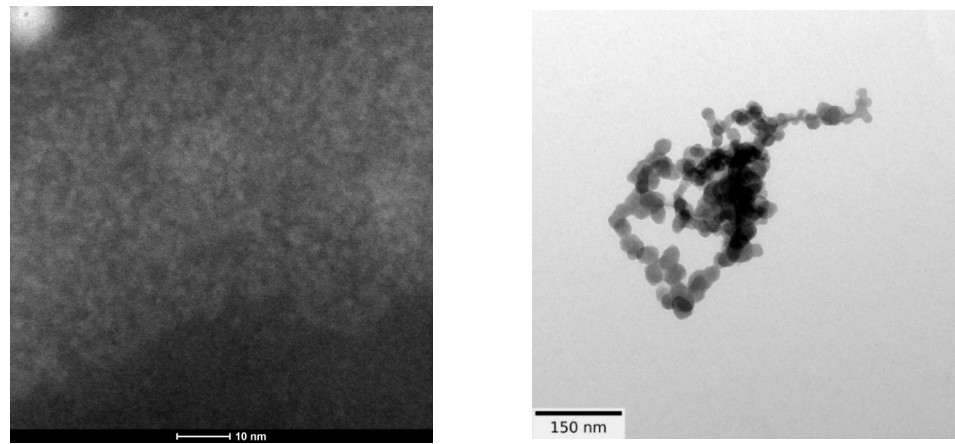


Figure 5. TEM images of dry fullerol (FD-C₆₀) (**left**) and 3HFWC (SD-C₆₀) (**right**). The fullerol molecule is about 1.3 nm in diameter, but under humidity, it may form agglomerates of different sizes (until hundreds nm) and shapes (linear, random foling, and balls). 3HFWC is a spherical molecule, about 15 nm in diameter (from 10 nm to 30 nm), and under humidity, it may form aggregates with dipole–dipole interactions.

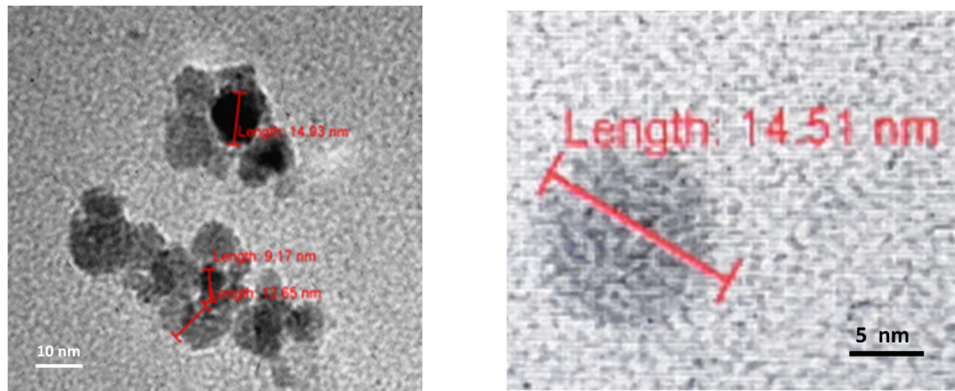


Figure 6. TEM images of the dry 3HFWC spherical molecule about 15 nm in size. In the center of the 3HFWC is fullerol (diameter 1.3 nm) surrounded by water shells (layers, average diameter 14.51–1.30 = 13.21 nm). Water molecules are ordered according to icosahedral three-dimensional Penrose tiling (3DPT) [22].

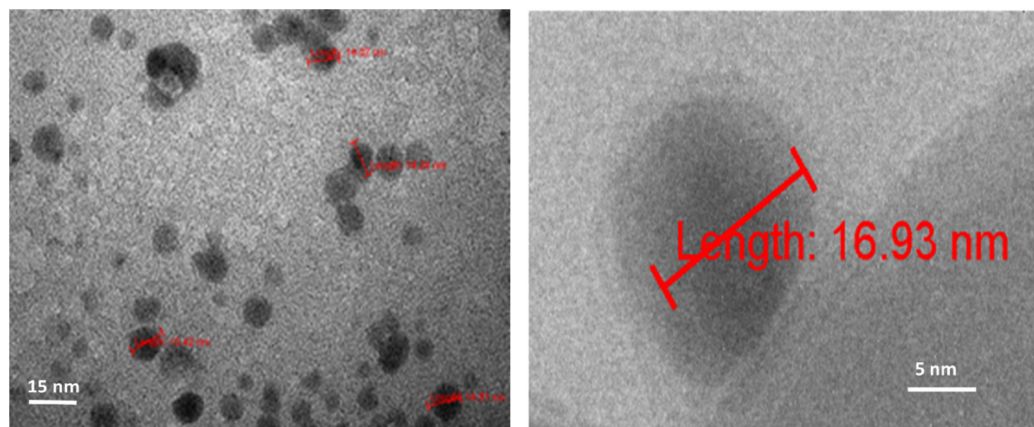


Figure 7. TEM images of dry 3HFWC spherical molecules about 17 nm in size. In the left image, the water shell has a diameter of 15.63 nm (16.93–1.30 = 15.63 nm), with the water molecules ordered according to three-dimensional Penrose tiling (3DPT) [22].

3.4. AFM/MFM Images

The results of AFM/MFM characterization of both dry substances, fullerol, and 3HFWC, are presented in Figures 8–12. Figure 8 shows four images of fullerol and 3HFWC. The pictures clearly show the dimensions, shape, and number of particles. Fullerol was most often organized as a dimer (size 2.6 nm, two molecules linked with water molecules from the humidity), while 3HFWC was seen as an individual particle with a size of about 15–30 nm.

High-resolution images of fullerol and 3HFWC are shown in Figure 9. With fullerol, in addition to dimers, organization into trimers could be seen, but in most cases, it formed a granular monomer structure. In the case of 3HFWC, spherical monomeric structures with a size of about 10–15 nm were clearly visible.

The exact value of 14.7 nm, one of several SD-C₆₀ (3HFWC) molecules, is shown in Figure 10. A similar size of 3HFWC was obtained from several TEM images, which indicated that the most frequently recorded size of SD-C₆₀ (3HFWC) was around 15 nm.

The result of a comparative examination of the presence of water in dried fullerol (FD-C₆₀) and dried 3HFWC (SD-C₆₀) using MFM (magnetic force microscopy) showed that fullerol contained a minimal number of water molecules originating from the humidity during the measurements (Figure 11), while 3HFWC had significantly more pronounced peak values and contained a significantly larger number of water molecules (Figure 12). The comparative presentation of the MFM values of fullerol and 3HFWC on one diagram is shown in Figure S3; they are in agreement with previously published results [22].

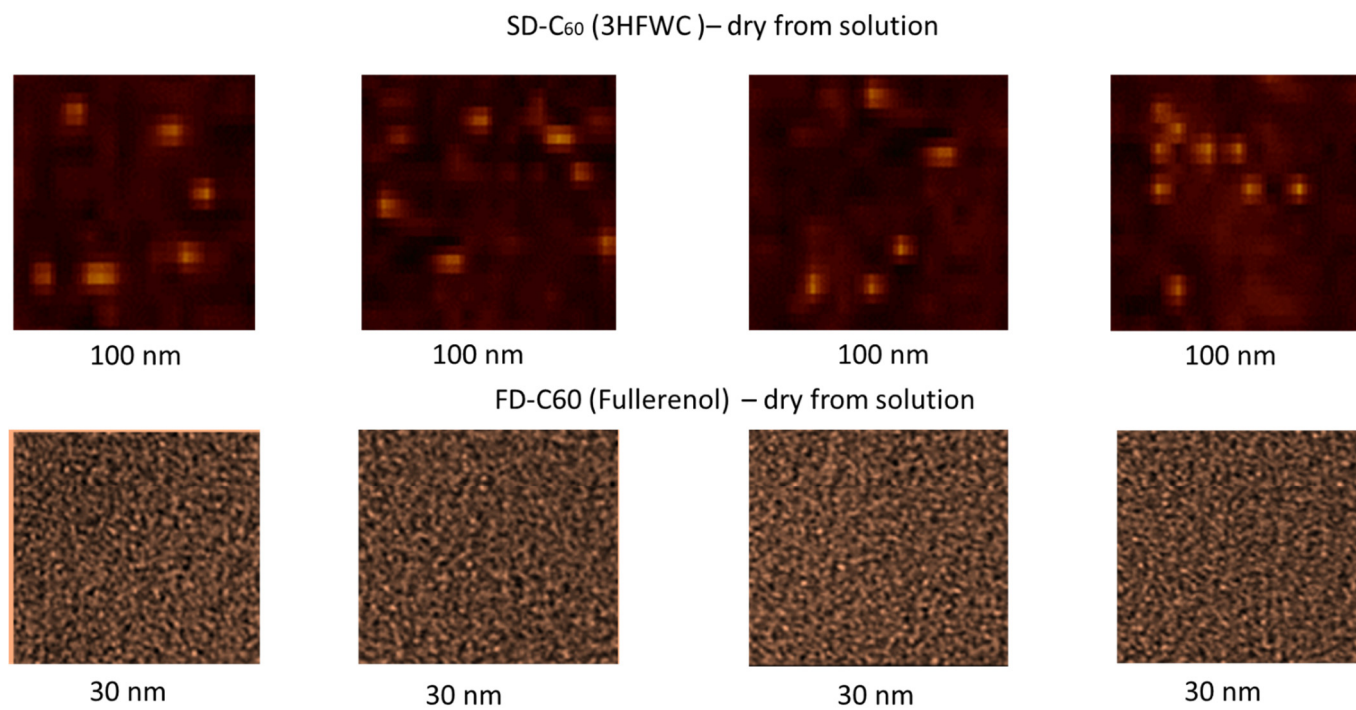


Figure 8. AFM/MFM images of dry 3HFWC (SD-C₆₀) and dry fullerol (FD-C₆₀), with four different scanning spots. The scanning surface of 3HFWC was 100 × 100 nm, while for fullerol it was 30 × 30 nm. Different scanning surfaces were chosen due to the different sizes of the two substances (fullerol is about 1.3 nm, while 3HFWC is between 10 and 30 nm). 3HFWC molecules were observed as separate structures (individual), while in the images of fullerol, individual molecules and smaller conglomerates were observed.

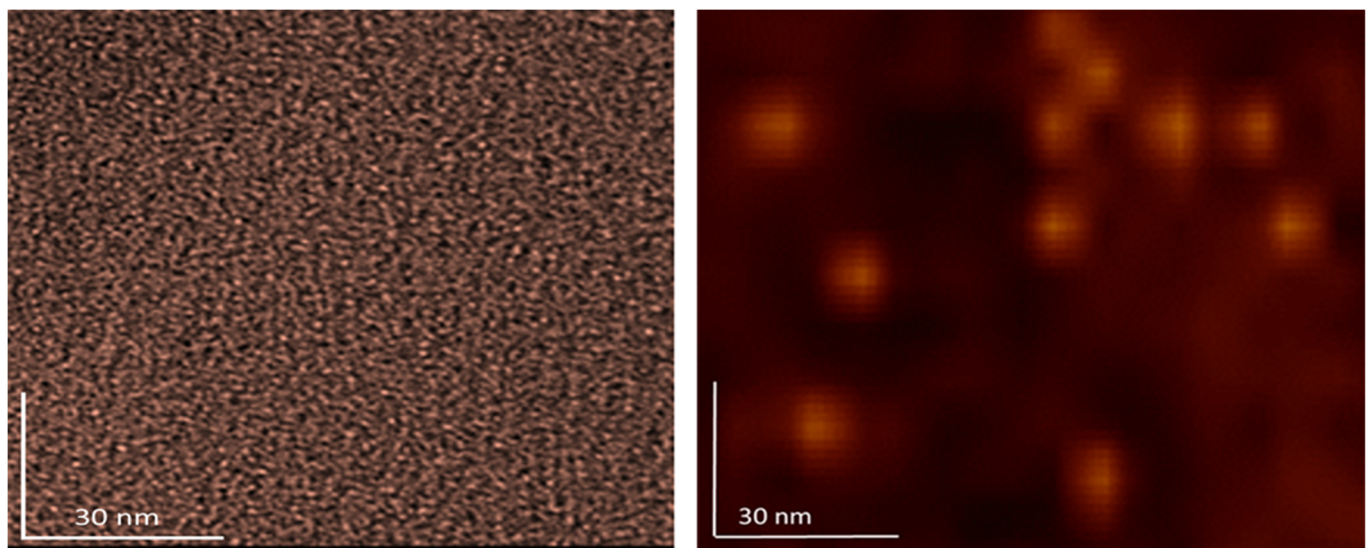


Figure 9. In order to clearly compare the sizes and organization of dry fullerol (**left**) and dry 3HFWC (**right**), the AFM/MFM images of the same scanning spots, 100×100 nm, were taken. As can be seen from the pictures, the differences in size and organization are different. As fullerol is a precursor to 3HFWC, they differ in their water layers, with thicknesses of 7 nm–14 nm forming around fullerol.

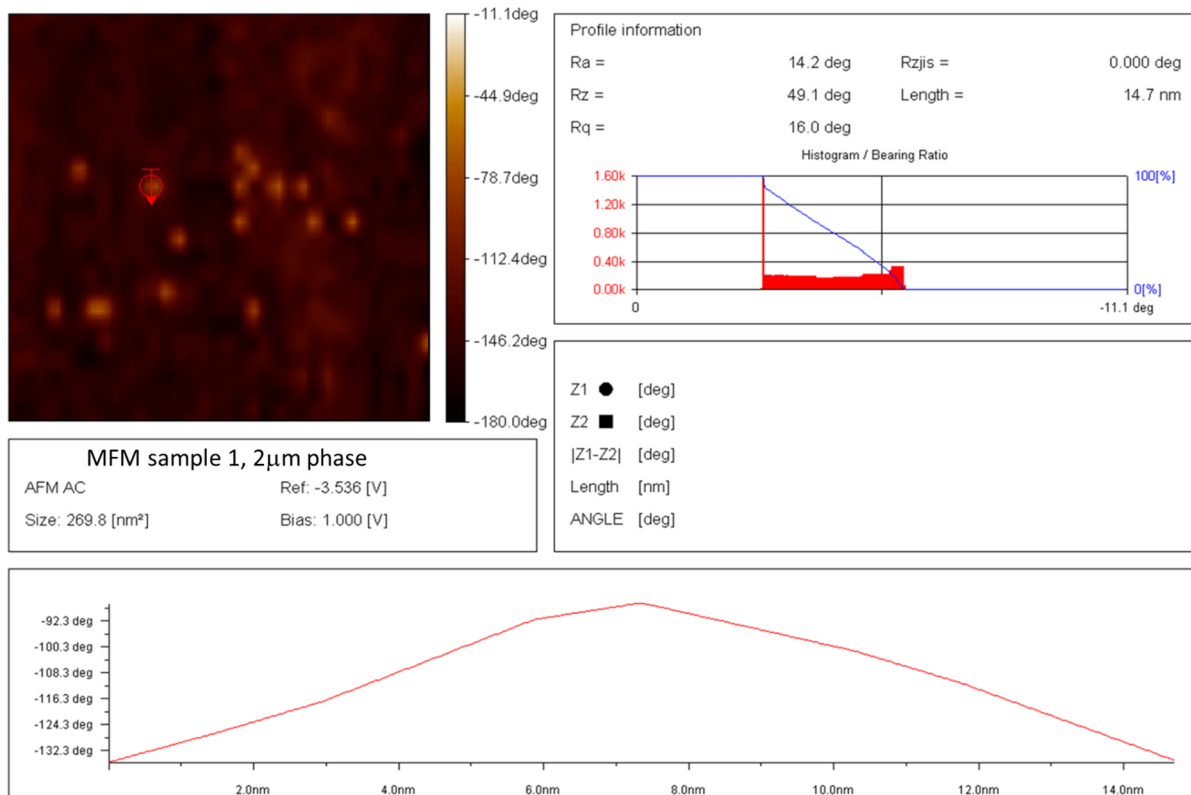


Figure 10. AFM/MFM image of dry 3HFWC with a scan area of 269.8 nm^2 , with 14 molecules of 3HFWC seen in the image. The molecular size of 3HFWC chosen for accurate measurement is 14.7 nm. As can be seen from the image, the surface of the molecules is not smooth (there are two subtle peaks at 5.9 nm and 7.4 nm), which is in agreement with previously obtained results [22].

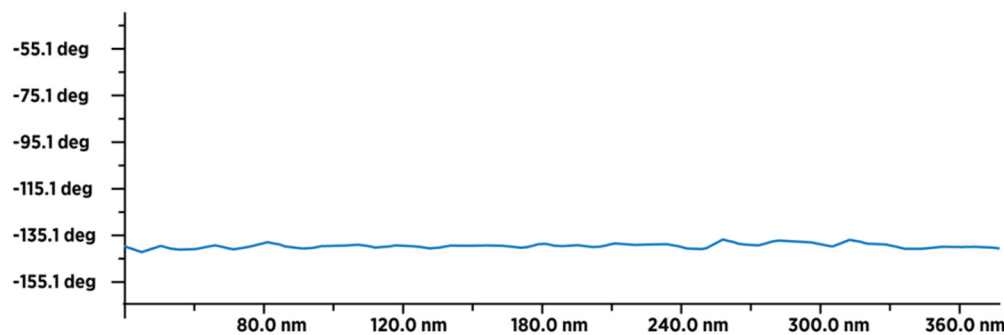


Figure 11. MFM image of 50–60 dry fullerenol molecules (in line) with an average type–sample interaction intensity of -140 degrees, which indicates that the sample is paramagnetic. The intensity and form of the graph indicate that a thin layer of humidity (water molecules) covered (evenly) the surface layer of fullerenol.

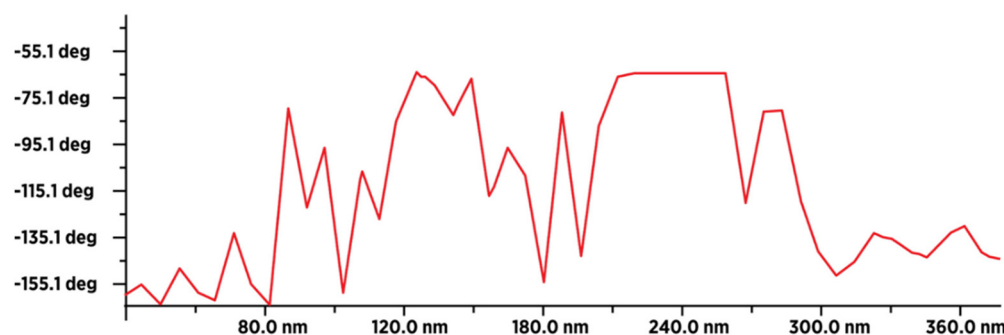


Figure 12. MFM image of about 18–20 dry 3HFWC molecules (in line) with an average type–sample interaction intensity of -100 degrees (minimum -165 degrees, and maximum -65 degrees), which indicates that the sample is less paramagnetic than fullerenol. This means that fullerenol, even if it has a smaller number of atoms (1.332 Da), has more unpaired electrons than 3HFWC, which has a significantly higher number of atoms (~ 3.200 Da). The intensity and form of the graph show that in addition to a thin layer of moisture, there are also water layers in 3HFWC (around fullerenol as the precursor to 3HFWC).

3.5. X-ray Diffraction (XRD)

Powder X-ray diffraction (XRD) was performed to see if there was a difference in the fullerenol and 3HFWC samples' structural order (Figure 13).

Fullerenol was used as delivered (yellow dust material) and additionally dried under vacuum (10 mbar/30 °C); 3HFWC was lyophilized to a powder prior to the measurement.

Both fullerenol and 3HFWC are hydrophilic. Lyophilized fullerenol is a molecular powder with interstitial water clusters formed from humidity. The XRD patterns of fullerenol showed broad Bragg peaks at 27–57° 2Theta due to partial crystallization of interstitial water. The higher water content (humidity + extra water) in 3HFWC induced a decrease in the reflex intensity and further broadened the reflexes. This indicated that the structure of 3HFWC was less ordered due to extra water molecules organized in aperiodic three-dimensional Penrose tilings with different “lattice” sizes (there are sixteen different tiling types [22]). The Penrose three-dimensional tiling pattern (3DPT) is a type of quasicrystal, which means that it has an ordered yet never-repeating structure.

However, it is precisely this organization that enabled SD-C₆₀ (3HFWC) to have exothermic properties at a temperature of 133 °C, while fullerenol had endothermic properties at 100 °C (Figures 14 and 15).

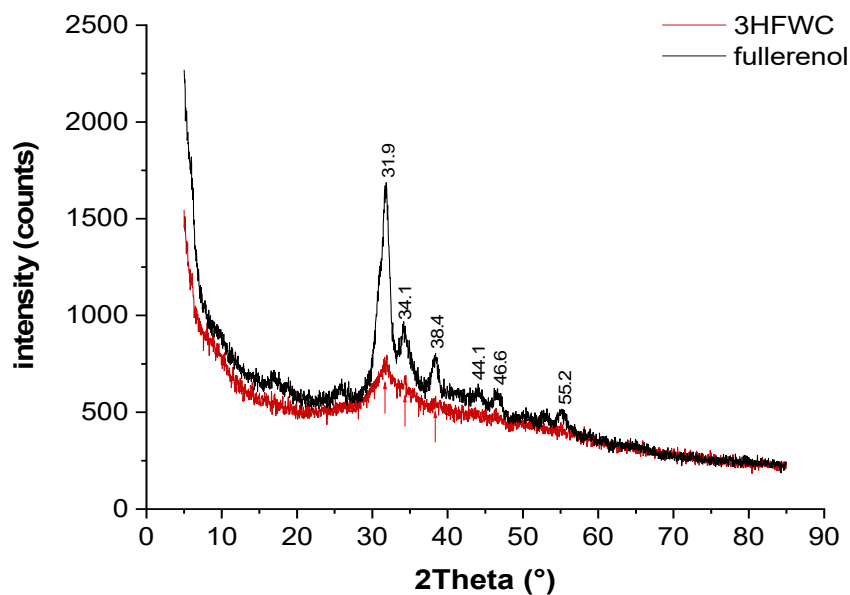


Figure 13. Powder XRD was performed to show the differences in the samples' structural order. The XRD patterns of fullerol show broad Bragg peaks at 27° – 57° 2Theta due to partial crystallization of interstitial water. The higher water content (humidity + extra water) in 3HFWC induced a decrease in the reflex intensity and further broadened the reflexes.

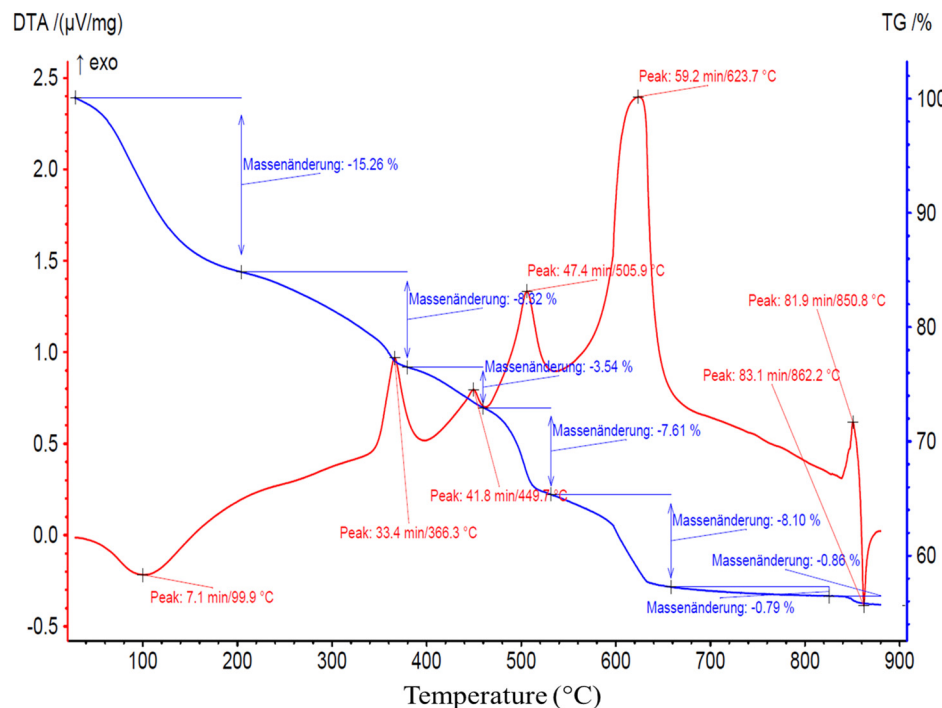


Figure 14. Fullerol (FD-C₆₀) TGA/DTA diagram with a peak at $99.9\text{ }^\circ\text{C}$ ($100\text{ }^\circ\text{C}$), thus indicating an endothermic reaction (water evaporation). Translation: Massenänderung—Mass change.

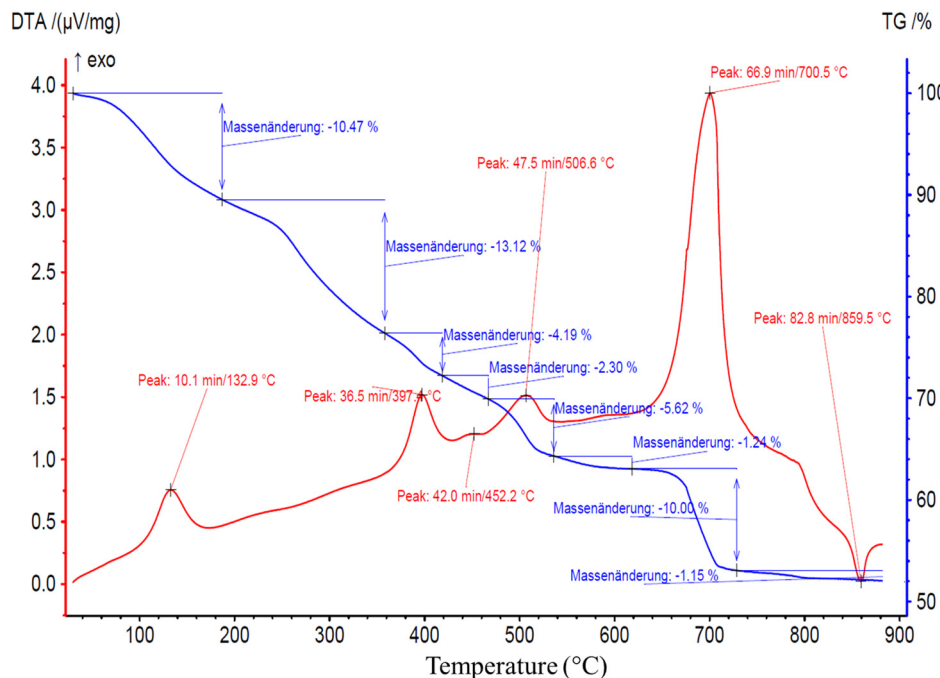


Figure 15. 3HFWC (SD-C₆₀) TGA/DTA diagram with a peak at 132.9 °C (133 °C), thus indicating an exothermic reaction (shifted to higher temperatures for evaporation). Translation: Massenänderung—Mass change.

3.6. TGA/DTA-MS-FTIR

Figures 14 and 15 show the results of the TGA/DTA measurements of fullerenol and 3HFWC, respectively. Since 3HFWC is proposed to be used as a cosmetic product, the focus in the interpretation of the results will be on temperature processes < 200 °C. In this temperature range, adsorbed solvents and water layers will be removed.

The mass loss of the fullerenol sample in the first mass loss step was 15.3 wt%. Taking into account that 3HFWC was freeze-dried at 0.37 mbar and 20 °C before measurement, it was noticeable that the mass loss up to approx. 200 °C was still high at 10.5 wt%. Interestingly, the corresponding DTA results of these processes show different enthalpies. While the first mass loss was an endothermic reaction in the fullerenol sample, 3HFWC showed an exothermic reaction. Additionally, the maximum of the DTA process was shifted to a higher temperature in 3HFWC. While the DTA peak in the endothermic process of fullerenol was at 100 °C, the maximum peak of 3HFWC was located at 133 °C.

TGA showed the mass loss of a sample during heating and sample decomposition, while DTA showed whether the single decomposition processes are of an endo- or exothermic nature. Exothermic reactions release energy, while endothermic processes, like the evaporation of solvents, need additional energy to be initiated. Thus, DTA measurements can indicate differences in the binding ratios of different substances during their decomposition.

Thermogravimetric analysis (TGA) and differential thermo analysis (DTA) coupled with mass spectrometry (MS) and infrared spectroscopy (FTIR) were performed on 3HFWC to identify any differences in the water layer bonding.

Both MS and FTIR demonstrated the release of water at temperatures below 200 °C under synthetic air conditions. 3HFWC released water in an exothermic reaction, while fullerenol released water in an endothermic reaction. Under the same sample treatment in a vacuum, differences in the reaction enthalpies, while releasing water, were obtained.

Figure 16 shows the FTIR spectra of fullerenol at 100 °C and 3HFWC at 133 °C during the DTA signal's maximum. In the case of MS (Figure 17), the *m/z* fragments, which can be detected below 200 °C—17 (OH⁺), 18 (H₂O⁺), and 44 (CO₂⁺)—were plotted.

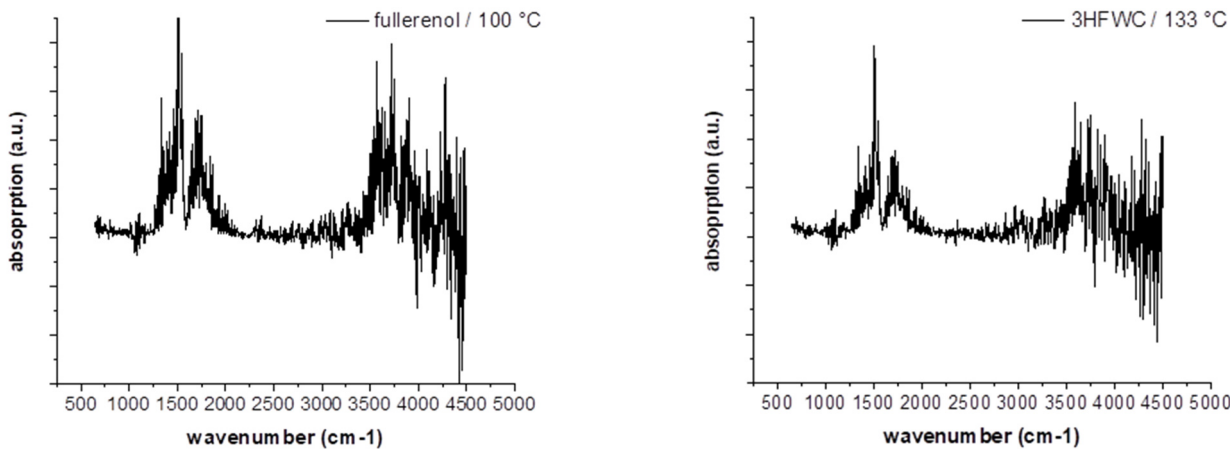


Figure 16. FTIR spectra of fullerol (FD-C₆₀) during the first endothermic DTA process at 100 °C (**left**) and 3HFWC (SD-C₆₀) during the first exothermic DTA process at 133 °C (**right**) in the TGA/DTA-MS-FTIR investigation.

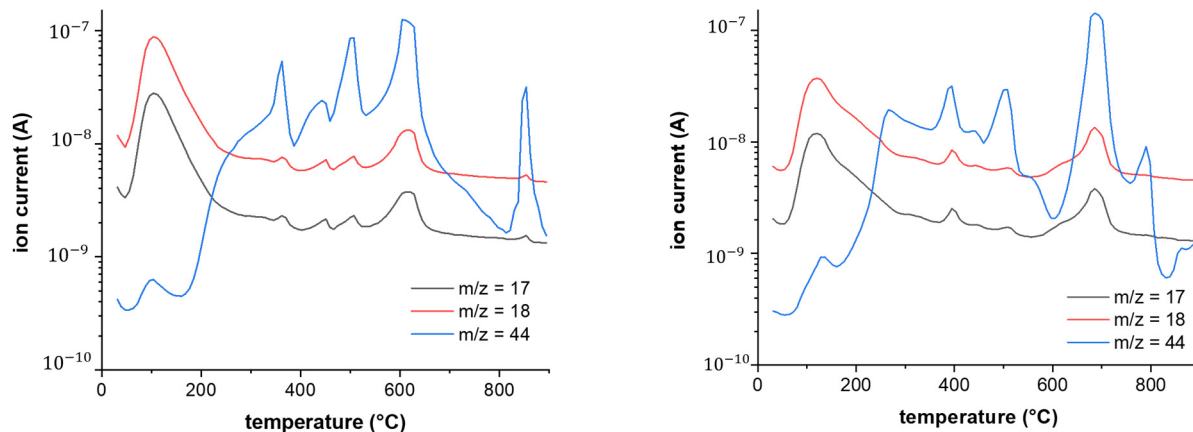


Figure 17. The MS spectra of fullerol (FD-C₆₀) at 100 °C (first endothermic DTA process) shows *m/z* fragments of 18 (H_2O^+) and 17 (OH^+), while signals of fragment 44 (CO_2^+) are very low at 100 °C (**left**). The MS spectra of 3HFWC (SD-C₆₀) at 133 °C (first exothermic DTA process) show *m/z* fragments of 18 (H_2O^+) and 17 (OH^+), while signals of fragment 44 (CO_2^+) are very low at 133 °C (**right**).

FTIR only indicated a release of water, which was highlighted in the MS due to the high ion currents of *m/z* = 17 (OH^+) and 18 (H_2O^+). CO_2 (*m/z* = 44) was also released in small amounts, with an ion current of two potencies less ($10^{-9} \rightarrow 10^{-7}$).

The decomposition of 3HFWC and fullerol at higher temperatures (<800 °C) took place in a similar way, with a tendency that the DTA signals for 3HFWC shifted to slightly higher temperatures. This indicated a structural difference in the two samples and differences in the water layers of 3HFWC, since even with the same pre-treatment, the differences in reaction enthalpies can be seen.

As no additional bands and *m/z* fragments were detected in fullerol, water was also released from 3HFWC, and no further decomposition processes took place below 200 °C. Bearing in mind that 3HFWC released water in an exothermic reaction, water molecules were bonded to 3HFWC in a different way than in fullerol.

Interestingly, the last decomposition process at 850–860 °C showed an endothermic decomposition process of 3HFWC but an exothermic followed by an endothermic process in fullerol. These differences in decomposition behavior also indicated a structural difference in the samples.

3.7. GPC

The gel permeation chromatography (GPC) results of fullerol (FD-C₆₀) and 3HFWC (SD-C₆₀) and analysis of the UV signal at 250 nm are presented in Figure 18. Since fullerol was expected to exhibit UV activity, calculations of the molar mass distributions were only carried out for UV-active species. The peak areas of the refractive index (RI) signal of side components were analyzed as well. The peaks at the elution volumes of approx. 27 and 31 mL were presumed to be system peaks.

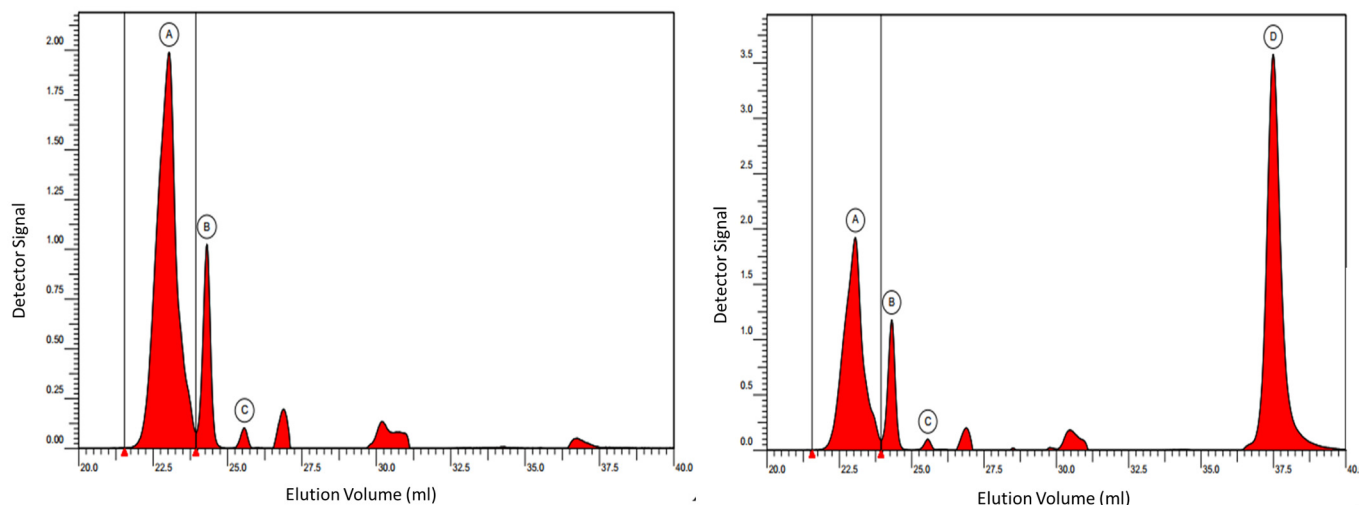


Figure 18. GPC fullerol diagram (**left**) with three peaks (A~2.00 a.u., B~1.00 a.u. and C~0.10 a.u.), and GPC diagram of 3HFWC (**right**) with four peaks (A, B, C with the same intensity as fullerol and a new peak D~3.5 a.u.). As can be seen, peak D intensity of 3HFWC (**right**) is dominant and much higher than peaks A, B, and C. Since fullerol is a precursor for 3HFWC synthesis, peaks A, B, and C exhibit the same intensity. Peak D in this case may only represent the water layers of 3HFWC.

A summary of the GPC results for 3HFWC were as follows: The peak area of fullerol showed three different separate peaks, while 3HFWC showed four different separate peaks. The relative content of each “species” and the molar mass at the peak maximum, M_p , were different. Three peaks and their observed masses were within the calibration curve, while one (peak D) was out of the calibration curve. We assumed this was 3HFWC with water layers. The mass of the fourth peak (D) could not be determined, but it should be more hydrophilic than fullerol.

3.8. Zeta Potential

At the same concentration of C₆₀(OH)₃₆ (0.150 g/L) in water (pH = 6.24, conductivity 2.2 μ S/cm), the pH of the fullerol (FD-C₆₀) solution was 9.349, while the pH was 7.107 for the 3HFWC (SD-C₆₀) solution (Table 2).

Table 2. Zeta potential, pH, electrophoretic mobility, and conductivity of fullerol and 3HFWC (same concentration of C₆₀(OH)₃₆, 0.150 g/L, in both the fullerol and 3HFWC solutions).

Test Substance	Temperature (°C)	pH	Zeta Potential (mV)	Electrophoretic Mobility (μ m/s)/(Vcm)	Conductivity (μ S/cm)
Fullerol (FD-C ₆₀)	25	9.35	-25.85 ± 1.71	-2.01 ± 0.13	0.18
3HFWC (SD-C ₆₀)	25	7.11	-43.29 ± 1.23	-3.37 ± 0.10	0.17
Difference	0	2.24	-17.44	-1.36	0.01

The zeta potential (ZP) value is a very important criterion for discerning the stability of a substance (Figure S7). The ZP of fullerol was -25.85 mV , while for 3HFWC, it was -43.29 mV , thus indicating that 3HFWC is more stable than fullerol. These findings clearly underline the difference between 3HFWC and its precursor (fullerol) (Table 2).

The zeta potential (electrostatic charge) of 3HFWC was higher than that of fullerol at an equivalent concentration. This was due to the hydration shells of water surrounding the fullerol molecules having more ordered bonding and, thus, greater polarity. This explains the stability of 3HFWC, possessing a greater electrostatic charge, greater electrostatic repulsion between 3HFWC molecules, and less agglomeration/sinking.

4. Discussion and Conclusions

Characterization of fullerol (FD-C₆₀) and 3HFWC (SD-C₆₀) in solution at a temperature of $20 \pm 1\text{ }^{\circ}\text{C}$ using NIR and FTIR spectroscopy showed differences in the spectra between the two substances within the 2500–3300 nm (NIR) and 2500–14,000 nm (FTIR) ranges. Using NIR spectroscopy, in addition to atmospheric pressure and a temperature of $20\text{ }^{\circ}\text{C}$, for 3HFWC (SD-C₆₀), spectra were run at temperatures of $80\text{ }^{\circ}\text{C}$, $90\text{ }^{\circ}\text{C}$, $120\text{ }^{\circ}\text{C}$, and $140\text{ }^{\circ}\text{C}$ (Figure S8). The obtained results indicated that at temperatures between $120\text{ }^{\circ}\text{C}$ and $140\text{ }^{\circ}\text{C}$, the water layers evaporate, i.e., the non-covalent hydrogen bonds are broken. The exact temperature that hydrogen bond breaking occurs was identified by the TGA/DTA tests. For 3HFMC, this happened at a temperature of $132.9\text{ }^{\circ}\text{C}$ ($133\text{ }^{\circ}\text{C}$), while for fullerol, evaporation (moisture) happened at $100\text{ }^{\circ}\text{C}$.

¹³C-NMR and ¹H-NMR showed clear structural differences of fullerol and 3HFWC. The absence of a peak on the ¹³C-NMR spectrum of 3HFWC could be interpreted in two ways. It may have been a weak signal (because only 1.1% of carbon atoms in nature are ¹³C); however, bearing in mind that we obtained clean signals with the same material in the form of fullerol, we suspect that it is possible that the water layers of 3HFWC may have absorbed the ¹³C signal. Since the difference in frequency between the water layers and ¹³C signal is of the order of $6(10^6)$, this opinion is based on the consideration of coupling at a high-frequency mode (O-H and O...H in water layers of 3HFWC, range $\sim 10^{14}\text{ Hz}$) and a low-frequency mode (resonant Larmor frequency for ¹³C, range 10^8 Hz) through their modulation of the amplitudes and phases. The general approach of nonlinear coupling (theoretical and experimental) of high- and low-frequency modes has been explained in the literature [54–62].

Additionally, the comparison of the FTIR signal intensity for C₆₀, fullerol, and 3HFWC (Table 3) indicated that the vibrational peaks of C₆₀ (with the corresponding shift) were present in both fullerol and 3HFWC; however, there was a big difference of up to seven times greater when it came to 3HFWC. The difference in the peak intensity between C₆₀ and fullerol was almost non-existent. To confirm the absence of a ¹³C-NMR signal for 3HFWC and explain the differences in the FTIR spectra of C₆₀, fullerol, and 3HFWC, additional extensive research is needed, which we intend to carry out in the near future.

Table 3. Wavelength shift and difference in the peak intensities of C₆₀ [46], fullerol (Figure 1) and 3HFWC (Figure 2) in the 7000–9000 nm FTIR range.

	Peak	C ₆₀	Fullerol	C ₆₀ /Fullerol (Shift/Difference)	3HFWC	C ₆₀ /Fullerol (Shift/Difference)
1.	Wavelength (nm)	7.003	6.370	633	7.340	337
	Intensity (a.u.)	0.192	0.190	0.002	0.027	0.165
2.	Wavelength (nm)	8.453	7.555	898	8.220	665
	Intensity (a.u.)	0.210	0.178	0.032	0.028	0.150

Characterization of the dry 3HFWC substance using TEM was performed three times, in 2018, 2019, and 2023, in three independent laboratories (Supplementary Materials Table S2). The age of the substance ranged from several months to four years. In all cases, it was shown that the size of dry 3HFWC was on average 15 nm depending on the number of

water layers it contained. The characterization of fullerenol was performed only once in 2023, and it was shown that the size was between 1.3 and 2.6 nm; in some cases, it was around 1 μm , which indicates that as soon as it comes into contact with moisture from the air it forms aggregates. Similar results were obtained with AFM/MFM characterization. 3HFWC was observed as a one-body object of size 10–30 nm. Fullerenol as a one-body object was 1.2–1.4 nm and from 2.5 to 6.0 nm as aggregates. The magnetic force microscopy spectra of 3HFWC and fullerenol were different. Since the intensity of the magnetic spectra is proportional to number of dipole–dipole interactions, it means that 3HFWC is richer with molecules which possess dipoles (water in layers) than fullerenol (only water from humidity). The possibility of characterizing various types of materials at the nano level, including biomaterials, using MFM has been reviewed in ref. [63–68].

Stability and pH values are important for substances that are used in biomedicine and cosmetics. The zeta potential of the 3HFWC substance was -43.29 mV , which indicates that it is very stable, while fullerenol had a value of -25.85 mV , which indicates that it is at the limit of its stability. Additionally, there was a difference in pH values, with 9.35 for fullerenol and 7.11 for 3HFWC.

In this paper, a contradiction regarding the degree of the structural order of fullerenol and 3HFWC obtained using $^1\text{H-NMR}$ and XRD was explained. When the order of protons in the structure was observed, 3HFWC was more ordered than fullerenol. The reason for this lies in the possibility of O-H rotation in the C-O-H structure, thus permitting the hydrogen atom to occupy various positions. Bearing in mind that it possesses about 36 OH groups, the positions of the hydrogen atoms form a very complex system. However, with 3HFWC, this is not the case because all the hydrogen atoms in the precursor (fullerenol) and in the three-dimensional Penrose tiling (3DPT) are fixed. However, if these two structures are considered from the aspect of classical crystallography (XRD), then fullerenol has a more ordered structure than 3HFWC; this is because fullerenol is a molecular crystalline structure while 3HFWC is a quasi-crystalline molecular structure because 3DPT (in water layers) are aperiodically ordered.

The TGA/DTA-MS-FTIR measurements showed the release of water at temperatures below $200\text{ }^\circ\text{C}$ under synthetic air conditions. There were differences in the bonding and release of the water layers. 3HFWC released water (humidity water + extra water) in an exothermic reaction; fullerenol released water (humidity water) in an endothermic reaction. Under the same sample treatment in a vacuum, the differences in the reaction enthalpies when releasing water were obtained.

SD-C₆₀ (3HFWC: C₆₀(OH)₃₆@(H₂O)₁₄₄₋₂₂₅₂ + humidity) showed a different decomposition behavior under a synthetic air atmosphere compared to FD-C₆₀ (fullerenol: C₆₀(OH)₃₆ + humidity). The main differences were as follows: (1) 3HFWC showed an exothermic reaction at $133\text{ }^\circ\text{C}$ when releasing water, while (2) fullerenol showed an endothermic release of water at $100\text{ }^\circ\text{C}$. With one exception, all the decomposition steps were slightly shifted to higher temperatures. The exception was the last exothermic process, which was shifted to lower temperatures for 3HFWC.

In summary, the core result was that water is bound in a different way in SD-C₆₀ (3HFWC) than in FD-C₆₀ (fullerenol), and fullerenol and 3HFWC are two different substances in terms of their structure, size, and physicochemical properties. The experimental results obtained in this research using various techniques (Section 2) showed that SD-C₆₀ (3HFWC) is a substance with excellent potential application in both cosmetics and pharmaceuticals. This new active ingredient acts biophysically through the vibrational modes of the hydrogen bonds in water and biomolecules, thus significantly affecting the conformational states of biomolecules. If the conformational states of biomolecules are diverse, the vibrational effects of SD-C₆₀ (3HFWC) will restore them to their normal original state.

Experiments on the application of fullerenol and 3HFWC in biomedicine have been reported, but there are no comparative studies in which the number of OH groups is the same in fullerenol (FD-C₆₀) and 3HFWC (SD-C₆₀). As in this paper, we plan to research

both substances with the same number of OH groups, as this is the only way to be sure of the differences in their effects on biological systems in vitro and in vivo.

Supplementary Materials: The following supporting information can be downloaded at: <https://www.mdpi.com/article/10.3390/nano14050480/s1>, Table S1: Icosahedral symmetry group. Table S2: Characterization of dry 3HFWC in five independent institutions. Figure S1: Fullerol OH group determination. Figure S2: Structural order of fullerol and 3HFWC. Figure S3: Water presence in fullerol and 3HFWC. Figure S4: Zeta potential of fullerol and 3HFWC. Figure S5: NIR spectrum of 3HFWC at different temperatures. References [69–72] are cited in Supplementary Materials.

Author Contributions: Investigation, visualization, formal analysis, and writing—original draft preparation and editing, D.K. (Djuro Koruga) and L.M.; investigation, formal analysis, I.S., D.K. (Dietmar Kuhn), B.C. and V.P.; conceptualization, supervision, formal analysis, data curation, and writing—review and editing, D.K. (Djuro Koruga); conceptualization, methodology, resources, and writing—review and editing, L.M.; supervision, formal analysis, data curation, writing—review and editing, funding acquisition, D.K. (Dietmar Kuhn), B.D.W. and S.D.; substance manufacturing and project administration, J.J. and N.J. All authors have read and agreed to the published version of the manuscript.

Funding: Grant number No.: 451-03-47/2023-01/200007, 3 February 2023, the Ministry of Science, Technological Development and Innovation of the Republic of Serbia and Faculty of Mechanical Engineering University of Belgrade, Contract research project No.: MF/TFT-01/23, 15 January 2023, Zepter International, Belgrade, Serbia; Faculty of Mechanical Engineering University of Belgrade; Contract research project No.: 22032914G860, 8 July 2022, BIOCOPTRON, AG, Switzerland, and LAUS GmbH, Germany; Contract research project No.: 2023-3760-140-45-00533-11, 24 April 2023, BIOCOPTRON, AG, Switzerland, and Fraunhofer-Institut für silicatforschung ISC, Germany.

Data Availability Statement: Data are contained within the article and its Supplementary Materials.

Acknowledgments: The first author (D.K.) would like to thank Aleksandra Korać and her co-workers, the Faculty of Biology, University of Belgrade, Serbia, for their collaboration and first electron microscopy images of 3HFWC. Zoran Mitrović, ProTech, d.o.o, Belgrade, Serbia, for his cooperation within Nano World, Belgrade, Serbia, in building the first reactor for the production of SD-C₆₀, as well as building together with Dušan Ječmenica, Metalelektrik, Belgrade, Serbia, with the financial support of Zepter International, Belgrade, Serbia, the second reactor for the commercial production of 3HFWC within the TFT Nano Center, Belgrade, Serbia. Additionally, many thanks to the operators for the production of SD-C₆₀ (3HFWC) within the TFT Nano Center. Marija Slavković, Nenad Jevtić, Nataša Knežević, Zorana Jović, Milica Paunović, and Jelena Janać for their assistance in the biomedical studies and administration of the TFT Nano Center in the period 2018–2023. The authors would like to thank Philipp Müller, Analytical and Material Science, the University in Heidelberg, Germany, for his collaboration in the characterization of fullerol (FD-C₆₀) and 3HFWC (SD-C₆₀) using TEM and NMR.

Conflicts of Interest: Author Djuro Koruga was employed as an entrepreneur researcher by the company NanoWorld. Author Dietmar Kuhn was employed by the company LAUS GmbH. Authors Nenad Jevtić and Jelena Janać were employed by the company TFT Nano Centre and author Bart De Wever was employed as an entrepreneur training by the company Altexa Development. The remaining authors declare that the research was conducted in the absence of any commercial or financial relationships that could be construed as a potential conflict of interest.

References

1. Osawa, E. Cornannulene. *Kagaku* **1970**, *25*, 854.
2. Kroto, H.W.; Heath, J.R.; O'Brien, S.C.; Curl, R.F.; Smalley, R.E. C₆₀: Buckminsterfullerene. *Nature* **1985**, *318*, 162. [[CrossRef](#)]
3. Krätschmer, W.; Lowell, D.; Fostiropoulos, L.K.; Huffman, D.R. Solid C₆₀: A new form of carbon. *Nature* **1990**, *347*, 354–358. [[CrossRef](#)]
4. Koruga, D.; Simic-Krstic, J.; Trifunovic, M.; Jankovic, S.; Hameroff, S.; Withers, J.C.; Loutfy, R.O. Imaging Fullerene C₆₀ with atomic resolution using a scanning tunneling microscope. *Fuller. Sci. Technol.* **1993**, *1*, 93–100. [[CrossRef](#)]
5. Harter, W.G.; Weeks, D.E. Rotation-vibration spectra of icosahedral molecules. I. Icosahedral symmetry analysis and fine structure. *J. Chem. Phys.* **1989**, *90*, 4727–4743. [[CrossRef](#)]

6. Arndt, M.; Nairz, O.; Vos-Andreae, J.; Keller, C.; Van der Zouw, G.; Zeilinger, A. Wave–particle duality of C₆₀ molecules. *Nature* **1999**, *401*, 680–682. [[CrossRef](#)]
7. Kanaseki, T.; Kadota, K. The “vesicle in a basket”. *J. Cell Biol.* **1969**, *42*, 202–220. [[CrossRef](#)]
8. Ericson, R.O. Tubular pacing of spheres in biological fine structures. *Science* **1973**, *181*, 705–708.
9. Haddon, R.C. Magnetism of the carbon allotropes. *Nature* **1995**, *378*, 249–255. [[CrossRef](#)]
10. Chiang, L.Y.; Upasani, R.B.; Swirczewski, J.W. Process of Forming Polysubstituted Fullerenes. U.S. Patent 5,177,248, 5 January 1993.
11. Sayes, C.M.; Fortner, J.D.; Guo, W.; Lyon, D.; Boyd, A.M.; Ausman, K.D.; Tao, Y.J.; Sitharaman, B.; Wilson, L.J.; Hughes, J.B.; et al. The differential cytotoxicity of water-soluble fullerenes. *Nano Lett.* **2004**, *4*, 1881–1887. [[CrossRef](#)]
12. Isakovic, A.; Markovic, Z.; Todorovic-Markovic, B.; Nikolic, N.; Vranjes-Djuric, S.; Mirkovic, M.; Dramicanin, M.; Harhaji, L.; Raicevic, N.; Nikolic, Z.; et al. Distinct cytotoxic mechanisms of pristine versus hydroxylated fullerene. *Toxicol. Sci.* **2006**, *91*, 173–183. [[CrossRef](#)]
13. Bogdanović, G.; Kojić, V.; Đorđević, A.; Čanadanović-Brunet, J.; Vojinović-Miloradov, M.; Baltić, V.V. Modulating activity of fullerol C₆₀(OH)₂₂ on doxorubicin-induced cytotoxicity. *Toxicol. Vitr.* **2004**, *18*, 629–637. [[CrossRef](#)]
14. Jiao, F.; Liu, Y.; Qu, Y.; Li, W.; Zhou, G.; Ge, C.; Li, Y.; Sun, B.; Chen, C. Studies on anti-tumor and antimetastatic activities of fullerol in a mouse breast cancer model. *Carbon* **2010**, *48*, 2231–2243. [[CrossRef](#)]
15. Liu, Y.; Jiao, F.; Qiu, Y.; Li, W.; Qu, Y.; Tian, C.; Li, Y.; Bai, R.; Lao, F.; Zhao, Y.; et al. Immunostimulatory properties and enhanced TNF- α mediated cellular immunity for tumor therapy by C₆₀(OH)₂₀ nanoparticles. *Nanotechnology* **2009**, *20*, 415102. [[CrossRef](#)]
16. Yamawaki, H.; Iwai, N.; Saito, K.; Okada, M.; Hara, Y. Cytotoxicity of water-soluble fullerene in vascular endothelial cells. *Am. J. Physiol. Cell Physiol.* **2006**, *290*, C1495–C1502. [[CrossRef](#)]
17. Johnson-Lyles, D.N.; Peifley, K.; Lockett, S.; Neun, B.W.; Hansen, M.; Clogston, J.; Stern, S.T.; McNeil, S.E. Fullerol cytotoxicity in kidney cells is associated with cytoskeleton disruption, autophagic vacuole accumulation, and mitochondrial dysfunction. *Toxicol. Appl. Pharmacol.* **2010**, *248*, 249–258. [[CrossRef](#)]
18. Saathoff, J.G.; Inman, A.O.; Xia, X.R.; Riviere, J.E.; Monteiro-Riviere, N.A. In vitro toxicity assessment of three hydroxylated fullerenes in human skin cells. *Toxicol. Vitr.* **2011**, *25*, 2105–2112. [[CrossRef](#)]
19. Shimizu, K.; Kubota, R.; Kobayashi, N.; Tahara, M.; Sugimoto, N.; Nishimura, T.; Ikarashi, Y. Cytotoxic Effects of Hydroxylated Fullerenes in Three Types of Liver Cells. *Materials* **2013**, *6*, 2713–2722. [[CrossRef](#)]
20. Koruga, D. Composition of Matter Containing Harmonized Hydroxyl Modified Fullerene Substance. U.S. Patent 8,058,483 B2, 15 November 2011.
21. Koruga, D. Compositions Comprising Hyper Harmonised Hydroxyl Modified Fullerene Substances. International Patent WO 2021/110234 A1, 10 June 2021.
22. Matija, L.; Stanković, I.; Purić, M.; Miličić, M.; Maksimović-Ivanić, D.; Mijatović, S.; Krajanović, T.; Koruga, D. The Second Derivative of Fullerene C₆₀ (SD-C₆₀) and Biomolecular Machinery of Hydrogen Bonds: Water-Based Nanomedicine. *Micromachines* **2023**, *14*, 2152. [[CrossRef](#)]
23. Markelić, M.; Mojić, M.; Bovan, D.; Jelača, S.; Jović, Z.; Purić, M.; Koruga, D.; Mijatović, S.; Maksimović-Ivanić, D. Melanoma Cell Reprogramming and Awakening of Antitumor Immunity as a Fingerprint of Hyper-Harmonized Hydroxylated Fullerene Water Complex (3HFWC) and Hyperpolarized Light Application In Vivo. *Nanomaterials* **2023**, *13*, 372. [[CrossRef](#)]
24. Markelić, M.; Draća, D.; Krajanović, T.; Jović, Z.; Vuksanović, M.; Koruga, D.; Mijatović, S.; Maksimović-Ivanić, D. Combined Action of Hyper-Harmonized Hydroxylated Fullerene Water Complex and Hyperpolarized Light Leads to Melanoma Cell Reprogramming In Vitro. *Nanomaterials* **2022**, *12*, 1331. [[CrossRef](#)]
25. Perovic, M.; Ciric, J.; Matovic, V.; Srbovan, M.; Koruga, D.; Kanazir, S.; Ivkovic, S. The presymptomatic treatment with 3HFWC nanosubstance decreased plaque load in 5XFAD mouse model of Alzheimer’s disease. *CNS Neurosci. Ther.* **2023**; *online ahead of print*. [[CrossRef](#)]
26. Lazovic, J.; Zopf, L.M.; Hren, J.; Gajdoš, M.; Slavkovic, M.; Jovic, Z.; Stankovic, I.; Matovic, V.; Koruga, D. Fullerene-Filtered Light Spectrum and Fullerenes Modulate Emotional and Pain Processing in Mice. *Symmetry* **2021**, *13*, 2004. [[CrossRef](#)]
27. Subotić, A.; Jevremović, S.; Milošević, S.; Trifunović-Momčilov, M.; Đurić, M.; Koruga, D. Physiological Response, Oxidative Stress Assessment and Aquaporin Genes Expression of Cherry Tomato (*Solanum lycopersicum* L.) Exposed to Hyper-Harmonized Fullerene Water Complex. *Plants* **2022**, *11*, 2810. [[CrossRef](#)]
28. Miljkovic, S.; Jeftic, B.; Stankovic, I.; Stojiljkovic, N.; Koruga, D. Mechanisms of skin moisturization with hyperharmonized hydroxyl modified fullerene substance. *J. Cosmet. Dermatol.* **2021**, *20*, 3018–3025. [[CrossRef](#)]
29. Miljkovic, S.; Jeftic, B.; Sarac, D.; Matovic, V.; Slavkovic, M.; Koruga, D. Influence of hyper-harmonized fullerene water complex on collagen quality and skin function. *J. Cosmet. Dermatol.* **2020**, *19*, 494–501. [[CrossRef](#)]
30. Serda, M.; Szewczyk, G.; Krzysztyńska-Kuleta, O.; Korzuch, J.; Dulski, M.; Musioł, R.; Sarna, T. Developing [60]Fullerene Nanomaterials for Better Photodynamic Treatment of Non-Melanoma Skin Cancers. *ACS Biomater. Sci. Eng.* **2020**, *6*, 5930–5940. [[CrossRef](#)]
31. Castro, E.; Garcia, A.H.; Zavala, G.; Echegoyen, L. Fullerenes in Biology and Medicine. *J. Mater. Chem. B* **2017**, *5*, 6523–6535. [[CrossRef](#)]
32. Kamat, J.P.; Devasagayam, T.P.; Priyadarsini, K.I.; Mohan, H. Reactive oxygen species mediated membrane damage induced by fullerene derivatives and its possible biological implications. *Toxicology* **2000**, *155*, 55–61. [[CrossRef](#)]

33. Mroz, P.; Pawlak, A.; Satti, M.; Lee, H.; Wharton, T.; Gali, H.; Sarna, T.; Hamblin, M.R. Functionalized fullerenes mediate photodynamic killing of cancer cells: Type I versus Type II photochemical mechanism. *Free. Radic. Biol. Med.* **2007**, *43*, 711–719. [[CrossRef](#)]
34. Franskevych, D.; Palyvoda, K.; Petukhov, D.; Prylutskaya, S.; Grynyuk, I.; Schuetze, C.; Drobot, L.; Matyshevska, O.; Ritter, U. Fullerene C₆₀ Penetration into Leukemic Cells and Its Photoinduced Cytotoxic Effects. *Nanoscale Res. Lett.* **2017**, *12*, 40. [[CrossRef](#)]
35. Bakry, R.; Vallant, R.M.; Najam-Ul-Haq, M.; Rainer, M.; Szabo, Z.; Huck, C.W.; Bonn, G.K. Medicinal applications of fullerenes. *Int. J. Nanomed.* **2007**, *2*, 639–649.
36. Anilkumar, P.; Lu, F.; Cao, L.; Luo, P.G.; Liu, J.-H.; Sahu, S.; Li, K.N.T.; Wang, Y.; Sun, Y.-P. Fullerenes for applications in biology and medicine. *Curr. Med. Chem.* **2011**, *18*, 2045–2059. [[CrossRef](#)]
37. Andrievsky, G.V.; Bruskov, V.I.; Tykhomirov, A.A.; Gudkov, S.V. Peculiarities of the antioxidant and radioprotective effects of hydrated C₆₀ fullerene nanostuctures in vitro and in vivo. *Free. Radical. Biol. Med.* **2009**, *47*, 786–793. [[CrossRef](#)]
38. Sharma, S.K.; Chiang, L.Y.; Hamblin, M.R. Photodynamic therapy with fullerenes in vivo: Reality or a dream? *Nanomedicine* **2011**, *6*, 1813–1825. [[CrossRef](#)]
39. Semenov, K.N.; Charykov, N.A.; Postnov, V.N.; Sharoyko, V.V.; Vorotyntsev, I.V.; Galagudza, M.M.; Murin, I.V. Fullerols: Physicochemical properties and applications. *Prog. Solid State Chem.* **2016**, *44*, 59–74. [[CrossRef](#)]
40. Semenov, K.N.; Andrusenko, E.V.; Charykov, N.A.; Litasova, E.V.; Panova, G.G.; Penkova, A.V.; Murin, I.V.; Piotrovskiy, L.B. Carboxylated fullerenes: Physico-chemical properties and potential applications. *Prog. Solid State Chem.* **2017**, *47–48*, 19–36. [[CrossRef](#)]
41. Vileno, B.; Marcoux, P.R.; Lekka, M.; Sienkiewicz, A.; Fehér, T.; Forró, L. Spectroscopic and photophysical properties of a highly derivatized C₆₀ fullerol. *Adv. Funct. Mater.* **2006**, *16*, 120–128. [[CrossRef](#)]
42. Guldi, D.M.; Prato, M. Excited-state properties of C₆₀ fullerene derivatives. *Acc. Chem. Res.* **2000**, *33*, 695–703. [[CrossRef](#)]
43. Kuhn, H.; Forsterling, H.-D. *Principles of Physical Chemistry*; John Wiley & Sons: Chichester, UK, 2000.
44. Kuzmany, H. *Solid State Spectroscopy*; Springer: Berlin/Heidelberg, Germany, 2009.
45. Hollas, J.M. *Modern Spectroscopy*; John Wiley & Sons: Chichester, UK, 1996.
46. Campbell, D.I.; Dwek, A.R. *Biological Spectroscopy*; The Benjamin/Cummings: Menlo Park, CA, USA, 1984.
47. Wiesendanger, R. *Scanning Probe Microscopy and Spectroscopy: Methods and Applications*; Cambridge University Press: Cambridge, UK, 1994.
48. Wolf, E.L. *Principles of Electron Tunneling Spectroscopy*; Oxford University Press: New York, NY, USA, 1985.
49. Kelsall, R.; Hamley, I.; Geoghegan, M. *Nanoscale Science and Technology*; John Wiley & Sons: Chichester, UK, 2005.
50. Vo-Dinh, T. (Ed.) *Nanotechnology in Biology and Medicine: Methods, Devices, and Applications*; CRC Press: Boca Raton, FL, USA, 2007.
51. Malsch, H.N. (Ed.) *Biomedical Nanotechnology*; CRC Press: Boca Raton, FL, USA, 2005.
52. Balci, M. *Basic 1H- and 13C-NMR Spectroscopy*; Elsevier BV: Amsterdam, The Netherlands, 2005; ISBN 9780444518118.
53. Luxbacherhe, T. *Zeta Potential for Solid Surface Analysis*; Anton Paar GmbH: Tokyo, Japan, 2014.
54. Anderson, T.; Nayfeh, A.; Balachandran, B. Coupling between High-Frequency Modes and a Low-Frequency Mode: Theory and Experiment. *Nonlinear Dyn.* **1996**, *11*, 17–36. [[CrossRef](#)]
55. Nayfeh, S.A.; Nayfeh, A.H. Energy transfer from high- to low-frequency modes in flexible structures via modulation. *J. Vib. Acoust.* **1994**, *116*, 203–207. [[CrossRef](#)]
56. Burton, T.D.; Kolowith, M. Nonlinear resonances and chaotic motion in a flexible parametrically excited beam. In Proceedings of the Second Conference on Non-Linear Vibrations, Stability, and Dynamics of Structures and Mechanisms, Blacksburg, VA, USA, 1–3 June 1988.
57. Pain, H.J. *The Physics of Vibrations and Waves*; John Wiley & Sons: Chichester, UK, 1999.
58. Hayashi, C. *Nonlinear Oscillations in Physical Systems*; MacGraw-Hill: Princeton, NJ, USA, 1964.
59. Biro, V. *Nonlinear Oscillations in Feedback Systems*; Akademiai Kiado: Budapest, Hungary, 1985.
60. Anderson, T.J.; Balachandran, B.; Nayfeh, A.H. Nonlinear Resonances in a Flexible Cantilever Beam. *J. Vib. Acoust.* **1994**, *116*, 480–484. [[CrossRef](#)]
61. Pai, P.F.; Nayfeh, A.H. A fully nonlinear theory of curved and twisted composite rotor blades accounting for warpings and three-dimensional stress effects. *Int. J. Solids Struct.* **1994**, *31*, 1309–1340. [[CrossRef](#)]
62. D'Alessandro, D. *Introduction to Quantum Control and Dynamics*; Chapman & Hall/CRC: Boca Raton, FL, USA, 2008.
63. Winkler, R.; Ciria, M.; Ahmad, M.; Plank, H.; Marcuello, C. A Review of the Current State of Magnetic Force Microscopy to Unravel the Magnetic Properties of Nanomaterials Applied in Biological Systems and Future Directions for Quantum Technologies. *Nanomaterials* **2023**, *13*, 2585. [[CrossRef](#)]
64. Shibata, N.; Findlay, S.D.; Kohno, Y.; Sawada, H.; Kondo, Y.; Ikuhara, Y. Differential phase-contrast microscopy at atomic resolution. *Nat. Phys.* **2012**, *8*, 611–615. [[CrossRef](#)]
65. Yang, Q.; Ma, Q.; Herum, K.M.; Wang, C.; Patel, N.; Lee, J.; Wang, S.; Yen, T.M.; Wang, J.; Tang, H.; et al. Array atomic force microscopy for real-time multiparametric analysis. *Proc. Natl. Acad. Sci. USA* **2019**, *116*, 5872–5877. [[CrossRef](#)]
66. Iturri, J.; Toca-Herrera, J.L. Characterization of Cell Scaffolds by Atomic Force Microscopy. *Polymers* **2017**, *9*, 383. [[CrossRef](#)]
67. Sergunova, V.; Leesment, S.; Kozlov, A.; Inozemtsev, V.; Platitsina, P.; Lyapunova, S.; Onufrievich, A.; Polyakov, V.; Sherstyukova, E. Investigation of Red Blood Cells by Atomic Force Microscopy. *Sensors* **2022**, *22*, 2055. [[CrossRef](#)] [[PubMed](#)]

68. Ares, P.; Jaafar, M.; Gil, A.; Gómez-Herrero, J.; Asenjo, A. Magnetic Force Microscopy in Liquids. *Small* **2015**, *11*, 4731–4736. [[CrossRef](#)] [[PubMed](#)]
69. Kettle, S.F.A. *Symmetry and Structure*; John Wiley and Sons: Chichester, UK, 1995.
70. Dresselhaus, M.S.; Dresselhaus, G.; Eklund, P.C. *Science of Fullerenes and Carbon Nanotubes*; Elsevier BV: Amsterdam, The Netherlands, 1996; ISBN 9780122218200.
71. Icke, V. *The Force of Symmetry*; Cambridge University Press: Cambridge, UK, 1995.
72. Hargittai, I. *Symmetry II: Unifying Human Understanding*; Pergamon Press: Oxford, UK, 1989.

Disclaimer/Publisher’s Note: The statements, opinions and data contained in all publications are solely those of the individual author(s) and contributor(s) and not of MDPI and/or the editor(s). MDPI and/or the editor(s) disclaim responsibility for any injury to people or property resulting from any ideas, methods, instructions or products referred to in the content.